Interaction of neutral vacancies and interstitials with the Si(001) surface

Taras A. Kirichenko,[1] Sanjay K. Banerjee,[1,*] and Gyeong S. Hwang[2,†]
[1]*Microelectronics Research Center, University of Texas, Austin, Texas 78713, USA*
[2]*Department of Chemical Engineering, University of Texas, Austin, Texas 78712, USA*
(Received 27 August 2003; revised manuscript received 24 November 2003; published 30 July 2004)

The interaction of neutral vacancies and interstitials with the clean Si(001) surface is studied using density functional theory calculations within the generalized gradient approximation. We find both vacancies and interstitials within topmost three subsurface layers are significantly stabilized by their strong interactions with the surface. Their formation energies are predicted to be a few eV lower than those at the bulk. This study suggests that a large fraction of neutral interstitials may reside in the subsurface layers. However, most vacancies will eventually remain in the form of missing dimers due to their significant formation energy difference. Along with structure and energetics, we analyze bonding of vacancies and interstitials based on electron density and electron localization function topologies. We also show the diffusion pathways and barriers of vacancies on the surface and at the subsurface layers.

DOI: 10.1103/PhysRevB.70.045321 PACS number(s): 68.35.Dv, 61.72.Bb, 66.30.−h, 31.15.Ew

I. INTRODUCTION

The geometry, dynamics, and electronic structure of intrinsic defects in semiconductors have been studied extensively because of their scientific interest and technological importance. The defects not only exhibit interesting physics of their own but also alter to a great extent the properties of materials. It is well known that the electrical and optical properties of semiconductors are governed by defects. In addition, surface chemical properties could be modified locally by surface and subsurface defects as well.

Many experimental and theoretical studies have been undertaken to understand the fundamental properties of vacancies and interstitials on the surface and in the bulk. However, little is known about the behavior of intrinsic defects at subsurface layers despite their importance particularly in better understanding their surface annihilation mechanisms. The Si(001) surface has been considered as an effective sink for bulk vacancies, but a detailed study of defect-surface interactions is still lacking. Surface annihilation of point defects is of great interest in ultrashallow junction formation for ever smaller semiconductor devices because it determines the concentration distribution of defects in the vicinity of the surface, which may, in turn, directly affect redistribution and electrical activation of injected dopant impurities.

In this paper, we examine the interactions of neutral vacancies and interstitials with the clean Si(001) surface using density functional slab calculations. First, we calculate the structure, energetics, chemical bonding, and diffusion of neutral vacancies on the clean surface and subsurface layers. Then, we look at the structure, energetics, and chemical bonding of neutral interstitials on the clean surface and its subsurface layers. The quantum theory of "atoms in molecules" (QTAM) (Refs. 1–6) is applied to investigating the bonding mechanism of these intrinsic defects.

II. COMPUTATIONAL DETAILS

All structures and energetics are calculated using the plane-wave-basis pseudopotential method within the generalized gradient approximation (GGA) (Refs. 9–11) to density functional theory (DFT),[7] as implemented in the Vienna *ab initio* Simulation Package (VASP).[8] We use Vanderbilt-type ultrasoft pseudopotentials.[12] A plane wave cutoff energy of 150 eV is used. We use a $2\times2\times1$ mesh of k points in the scheme of Monkhorst-Pack[13] for the Brillouin zone (BZ) sampling.

The structures and relative formation energies of vacancies and interstitials at subsurface layers reported herein are calculated using the ten-atomic layer (4×4) slab. The slab is separated from its vertical periodic images by a vacuum space of $\leqslant$15 Å. We have checked carefully the convergence of structure and energetics with respect to the slab thickness and the surface unit cell size [by increasing the thickness to thirteen layers and the surface cell size to (4×6)]. The comparison shows there is no significant change in structural properties and energetics with the slab thickness. Regarding the cell size, the difference between the (4×6) and the (4×4) surface cell for the relative energies of the surface and the first subsurface vacancies is only about 0.05 eV (well within the error of a DFT calculation), but the structural properties remain virtually unchanged. The convergence test confirms that our (4×4) model surface with ten-atomic layers is sufficient. The dynamics of vacancies on the clean surface is investigated using a five-layer (4×6) slab. The bottom layer Si atoms are fixed at the bulk position and their dangling bonds are passivated by H atoms. The remaining Si layers are fully relaxed using conjugate gradient method to minimize the total energy until all residual forces on the atoms become smaller than 5×10^{-2} eV/Å. Electron wave function optimization at each ionic iteration is performed using the residual minimization method (RMM) direct inversion in the iterative subspace (DIIS), with a convergence of 10^{-5}eV.

We calculate diffusion barriers and pathways using the nudged elastic band method (NEBM).[14,15] The NEBM starts by setting a chain of geometries (replicas) (interpolated between two local minima). A spring interaction between adjacent images is added to true ionic forces, thus mimicking an

elastic band. Then, projection ("nudging") of each force in the direction parallel and perpendicular to the path is performed and only the perpendicular component of the true ionic force and the parallel component of the spring force are included to the total force. While initial and final configurations are kept fixed the position of each intermediate image is adjusted to minimize the total force acting on the images. This allows a search for a minimum energy pathway between two local minima without putting any constrain on the atomic motion and without requiring any prior knowledge about a potential energy surface.

We apply the quantum theory of "atoms in molecules" (QTAM) (Ref. 16) to investigating the bonding mechanism of defective systems. From an analysis of the topological properties of electron densities, we could obtain an insight into the nature of bonding. Along with a charge density ρ and its gradient $\nabla\rho$, the Laplacian $\nabla^2\rho$ provides a physical basis for classification of atomic interactions. Particularly, the Laplacian maps show where electronic charge is locally concentrated, allowing one to identify bonding and nonbonding regions. A pair of bonded atoms can be connected by a unique line, along which charge density is maximal with respect to any lateral displacement (from the bond path). Such a line is referred to as the atomic interaction line (AIL). The local maxima of the $-\nabla^2\rho$ close to or far off AIL show correspondingly bonded or nonbonded charge concentrations.

Due to the lack of describing the Pauli exclusion principle, the charge-density topology analysis alone cannot explain an additional decrease in the excess local kinetic energy density (resulting from formation of electron pairs). Thus, the electron localization function (ELF) (Ref. 17) has been also employed in studying bonded interactions. ELF represents the electron pair localization in terms of the conditional probability of finding an electron in the neighborhood of another electron with the same spin. By definition, ELF ranges between 0 and 1, with perfect localization corresponding to 1. Typically relatively large values of ELF $\geqslant 0.5$ represent the regions of bonding and nonbonding localized electrons, whereas smaller values of <0.5 suggests the regions of delocalized electrons. Thus, ELF isosurface maps provide a clear picture for the positions of the bonding and nonbonding regions of localized electron pairs.

III. RESULTS AND DISCUSSION

It is well known that the surface atoms of Si(001) are dimerized to reduce the surface energy. At low temperatures ($<$200 K), the dimers appear to remain alternatively buckled along a dimer row, with antiphase correlation between dimer rows, leading to the well-ordered $c(4\times2)$ structure. The antiferromagnetic phase is widely accepted as the ground state of Si(001),[18] although a controversy still remains.[19] For the $c(4\times2)$ state, our DFT-GGA calculation yields the bond length of 2.31 Å and the buckling angle of 18.0°, in good agreement with previous DFT calculations.[20] In the following sections, we will present the structure, energetics and bonding of neutral vacancies and interstitials on the clean Si(001) surface and its subsurface layers.

TABLE I. Relative formation energy of a neutral vacancy at different subsurface layers with respect to the fifth layer vacancy whose formation energy is set to be zero.

			2		3		
Layer	0	2A	2B	3A	3B	4	5
Total energy change, eV	−2.4	−2.2	−2.0	−2.2	−1.5	−0.1	0.0

A. Neutral vacancies

1. Structure, energetics and chemical bonding

Figure 1(a) shows the $c(4\times2)$ reconstructed surface. Here atoms 1–6 belong to surface layer, atoms 7–14 to the first subsurface layer, atoms 15–18 to the second sublayer, and atoms 19–21 to the third sublayer. In Table I we summarize the change of total energy of the defective system with position of neutral vacancy. The total energy increases rapidly as the vacancy is moved into a deeper subsurface layer, and it levels off beyond the fourth subsurface layer. The large energy difference of 2.4 eV between the surface and the fourth layer vacancies suggests that neutral vacancies could be trapped (annihilated) near the surface.

First, we look at the structure and bonding of single vacancies on the Si(001)-$c(4\times2)$ surface. The up- and down-atom vacancies are constructed by removing the buckled up and down Si atoms, respectively. Figure 1(b) shows the relaxed configuration of the up-atom vacancy at the neutral state. For both the up- and down-atom vacancies, the second layer atoms [indicated as 12 and 13 in Fig 1(c)] around the vacancy undergo a significant inward relaxation to form the weak 12-13 bond with a distance of 2.82 Å.

For the up-atom vacancy, the remaining atom of the "defect" dimer moves upward by 0.39 Å. Thus, it appears that three consecutive dimers (including the defect dimer) are oriented in the same direction. The remaining atom is bonded to two subsurface atoms. The 2-8 and 2-9 back-bonds (2.34 Å) are noticeably shortened relative to the back-bonds (2.40 Å) of an up atom on clean Si(001). The centers of the ELF's and the Laplacian critical points are slightly displaced from the straight 2-8 or 2-9 paths, indicating the back-bonds are strained to some extent. Now we can expect that the remaining atom has a lone pair of electrons. [Indeed, as shown in Fig. 1(b), the ELF isosurface of nonbonding localized electrons appears to be larger than that of an upatom on the clean surface. Here, the value for all ELF isosurfaces is set to be 0.86.] The buckling of the next neighboring dimers gets weaker; that is, the buckling angle reduces from 18° to 14°. The buckling reduction leads to less charge transfer from the down atom to the up atom, which is well demonstrated by the reduced area of ELF isosurfaces for nonbonding localized electrons (on top of the up atoms). The down-atom vacancy formation is accompanied by the flipping of the next neighboring dimers, and thus five consecutive dimers (including the "defect" dimer) are buckled to the same orientation. The down-atom vacancy turns out to be as stable as the up atom vacancy. [The energy difference between them is

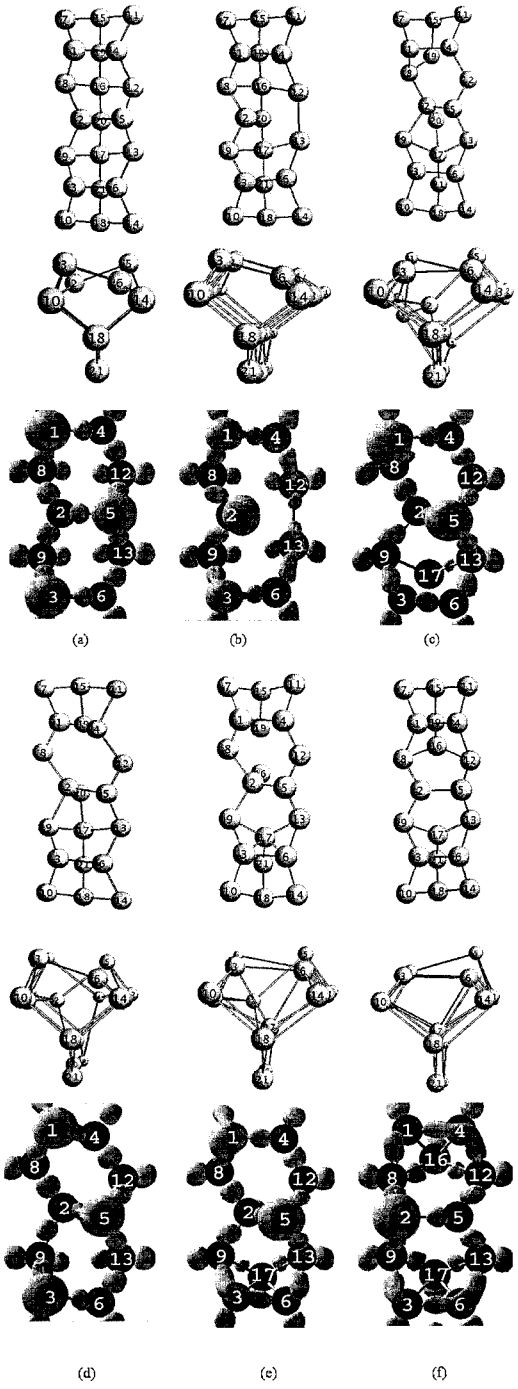

FIG. 1. (Color online) Top (top) and side (middle) view, together with ELF=0.86 isosurface maps (bottom), of surface and subsuface vacancy defect structures. (a) $c(4\times2)$ reconstructed clean Si(001) surface. (b) Up-atom surface vacancy: The atom 5 [from (a)] is removed. The bond lengths change to $d_{12\text{-}13}=2.82$ Å, $d_{2\text{-}8}=d_{2\text{-}9}=2.34$ Å, and $d_{1\text{-}4}=d_{3\text{-}6}=2.32$ Å. (c) Second layer vacancy at the state 2A. The atom 16 removed, resulting in $d_{2\text{-}20}=2.39$ Å, $d_{2\text{-}5}=2.36$ Å, $d_{2\text{-}8}=2.33$ Å, $d_{2\text{-}9}=2.47$ Å. (d) Second layer vacancy at the state 2B, with $d_{19\text{-}20}=3.87$ Å, $d_{1\text{-}4}=d_{2\text{-}5}=2.39$ Å. (e) Third layer vacancy at the state 3A. $d_{2\text{-}16}=2.43$ Å, $d_{1\text{-}8}=d_{4\text{-}12}=2.25$ Å. (f) Third layer vacancy at the state 3B, with $d_{1\text{-}4}=d_{3\text{-}6}=2.30$ Å and the distance between two fourth layer atoms (which were bonded to the removed atom 20) of 3.34 Å.

only 0.03 eV per (4×6) surface cell, well within the error of a DFT calculation.] We also check the effect of next neighboring rows by comparing the energy difference between the up and down atom vacancies from the $c(4\times2)$ and the $p(2\times2)$ surface cells. The energy difference is estimated to be less than 0.02 eV, suggesting the influence of neighboring rows is insignificant. We also examine an outward relaxation of the second layer atoms, as suggested by Low *et al.*[6] However, this configuration turns out to be 0.13 eV [per (4×6) unit cell] less favorable than the up-atom vacancy.

We also calculate the formation energy of a single missing dimer, which turns out to be 1.8 eV lower than two separated surface vacancies. The energy difference is quite similar to the energy gain by the vacancy-vacancy pairing in Si.[21] In fact, it is not surprising as the stabilization is mainly ascribed to the reduction of dangling bonds. This result clearly demonstrates that a single missing dimer is energetically far more stable than two separated surface vacancies.

Second, we look at single vacancy formation at the first subsurface layer[22] by removing the atom 8. Upon geometry optimization, the surface atom 1 slides down to the position of the removed atom 8, leading to a surface vacancy. This suggests that a vacancy at the first subsurface layer is unstable.

Third, we identify a very stable state (state 2A) of neutral vacancies at the second subsurface layer. The vacancy is created by removing the atom 16. Initially, four dangling bonds are created (at the atoms 8, 12, 19, and 20, around the vacancy). Upon geometry relaxation, as shown in Fig. 1(c), the surface atom 2 is greatly displaced downward. This leads to the formation of weak 2-20 and 8-19 bonds with distances of 2.39 and 2.54 Å, respectively. The 2-9 bond is significantly stretched to 2.47 Å (initially, 2.34 Å). As the atom 9 is dragged towards the atom 3, the up atom 3 is moved down and thus the 3-6 dimer is nearly symmetrized.

The atom 2 forms three covalent bonds with neighboring 5, 8, and 20 atoms that appear to exist nearly on the same plane, and also it barely exhibits a fourth close-shell interaction (with the atom 9). This suggests the surface atom 2 still retains the sp^2 hybridization. It is likely that some charge is transferred from the down atom 2 to the up atom 5. The atom 12 shows a characteristic of sp^2 hybridization; that is, it forms three covalent bonds that lie on a plane. A released electron from the atom 12 is delocalized, populating more negative charge at the adjacent dimers. The nonlocal effect has been found to be significant along a dimer row. Indeed, the sum of all bond angles of the up atom 5 is decreased from 281° to 264°, implying that the mixing ratio of the *s* orbital in the dangling bond is increased and the energy of the occupied states is decreased.

The vacancy state is energetically only 0.2 eV [per (4×4) surface cell] less stable than the surface vacancy. We attribute the stabilization to (i) reduction of dangling bonds in the subsurface layers and (ii) delocalization of electrons on the local surface.

We also identify a metastable vacancy (state 2B) at the second subsurface layer [Fig. 1(d)]. The 8-19 bond is now broken, and the weak 19-20 bond is formed by the Jahn-Teller distortion. The atoms 8 and 12 are three coordinated,

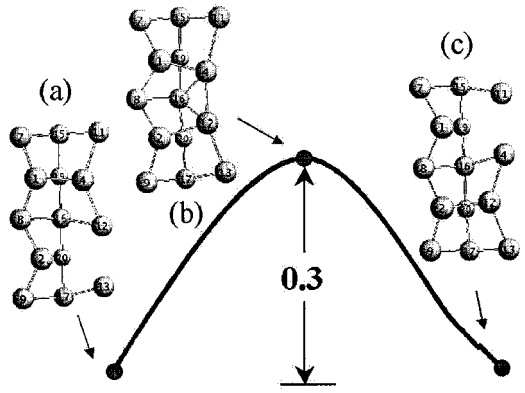

FIG. 2. (Color online) Pathway and energetics for neutral vacancy diffusion along the dimer row. (a) Initial state (up-atom vacancy), (b) transition state, and (c) final state (down-atom vacancy).

exhibiting sp^2 hybridization. The released electrons from the atoms 8 and 12 are again delocalized on the local region, which in turn lowers the total energy.

The vacancy (state 2B) is about 0.2 eV less favorable than another (state 2A) second layer vacancy (*vide supra*). No bond breakage is involved in the transformation from the state 2B to the state 2A. Thus, the energy barrier is minimal (*vide infra*). At elevated temperatures, we can therefore expect that the former can easily be converted to the latter.

Fourth, we look at vacancy formation at the third subsurface layer by removing the atom 20. The relaxed structure is shown in Fig. 1(e) (state 3A). Initially, four dangling bonds are created **(**at the atoms 16, 17, and two other atoms at the fourth subsurface layer [not shown in Fig. 1(e)]**)**. The surface atom 2 is significantly displaced downward to form the 2-16 bond (2.43 Å) while pushing the atom 16 down. This in turn leads to (i) breakage of 12-16 and 8-16 bonds and (ii) formation of bonds between 16 and fourth layer atoms (which were connected to the removed atom 20). As a result, the atoms 8 and 12 have a dangling bond, whereas the fourth layer atoms are four coordinated.

The atom 2 now shows a sp^3 characteristic, rather than sp^2. The atoms 8, 12, and 17 exhibit three normal covalent bonds that lie on a plane. The atom 17 also shows a fourth weak close-shell interaction (out of the plane, pointing to the center of the symmetrized 3-6 dimer.) It appears that released electrons from the atoms 8 and 12 are delocalized on the local surface. The 1-8 and 4-12 bond distances are about 2.25 Å, much shorter than 2.40 Å for corresponding back bonds of an asymmetric dimer on the clean surface. The stronger bonding interactions are well demonstrated by ELF [Fig. 1(e)] and charge and Laplacian density topology maps that exhibit more charge accumulation within the bonds. The third layer vacancy turns out to be very stable; its formation energy is only 0.2 eV larger than the surface vacancy and about 2.2 eV smaller than the fifth layer vacancy (which is assumed to be similar to a bulk vacancy).

We identify another stable configuration of neutral vacancies at the third layer (state 3B). Again, the atom 20 is removed. The relaxed structure is shown in Fig. 1(f). In this case, the surface atom 2 is insignificantly displaced and

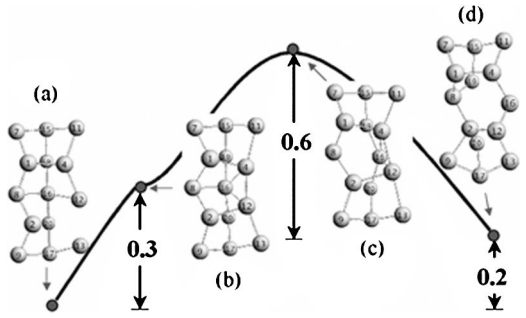

FIG. 3. (Color online) Pathway and energetics for neutral vacancy diffusion into the subsurface layer. (a) Initial state (up-atom vacancy), (b) intermediate saddle point, (c) transition state, (d) final state (subsurface vacancy).

retains the sp^2 hybridization. The 8-16 and 12-16 bonds are preserved. The atoms 16 and 17 undergo significant outward relaxation. The two fourth layer atoms (which were bonded to the removed atom 20) form a weak bond with a distance of 3.34 Å [not shown in Fig. 1(d)]. The 1-4 and 3-6 dimers are symmetrized.

The atoms 16 and 17 exhibit three normal covalent bonds that lie on a plane, and also show a fourth weak close-shell interaction (out of the plane, pointing to the center of the symmetrized 1-4 and 3-6 dimers, respectively). The *p*-like interactions are likely to stabilize the defective system substantially. The formation energy of the third layer vacancy is about 1.55 eV lower than that of the fifth layer one (which exhibits large pairing Jahn-Teller distortions, similar to a typical bulk vacancy[23–28] resulting in two weak bonds between the atoms around the vacancy). However, the 3B vacancy state is energetically less favorable than the 3A state shown earlier (in which the dangling bonds at the fourth layer are terminated by the atom 13). The transformation from the state 3B to the state 3A involves breakage of 8-16 and 12-16 bonds, leading to a relatively large energy barrier of 0.6 eV (*vide infra*).

Finally, we look at a neutral vacancy at the fourth and fifth subsurface layers. No significant changes arise in the surface structure, suggesting the vacancy-surface interaction is no longer significant. The fourth layer vacancy appears to be about 0.2 eV more stable than the fifth layer vacancy. The former exhibits the C_{2v}-point symmetry while the latter exhibits the D_{2d}-point symmetry. Note that the symmetry of a neutral vacancy at the bulk lowers from T_d to D_{2d} by the Jahn-Teller effect, although the change in formation energy is insignificant.[28] Here, the C_{2v} symmetry at the fourth layer is mainly due to the strain induced by surface reconstruction; that is, the fourth layer vacancy helps to relieve the sublayer strain to some extent, resulting in the formation energy lowering with respect to the fifth layer one.

2. Diffusion dynamics

In this section, we present the diffusion pathways and barriers of a neutral vacancy on the clean surface and its subsurface layers. First, we look at vacancy diffusion along a dimer row using the NEBM method. Figure 2 shows the

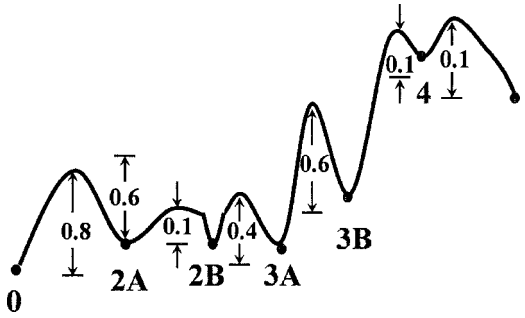

FIG. 4. (Color online) Energetics (in eV) along the diffusion pathway for a subsurface neutral vacancy. 0 denotes the surface vacancy, 2A and 2B indicate the second sublayer vacancy at the state A and B, respectively, 3A and 3B is the third sublayer vacancy at the A and B state, and 4 and 5 are the vacancy at the fourth and fifth subsurface layers.

initial (a), transition (b), and final (c) state configurations of the diffusing vacancy between two adjacent surface sites. The vacancy diffusion involves a consorted motion of two surface atoms (4 and 12). In the transition state, the atom 12 moves outward to interact with the remaining atom 2 while the atom 4 moves downward to form a weak bond with the third layer atom 16. The diffusion barrier is calculated to be 0.3 eV. The relatively low barrier indicates that the surface single vacancies are highly mobile at elevated temperatures. Vacancy-vacancy pairing by surface diffusion appears to be mainly responsible for single missing dimer formation,[29] rather than the liberation of the remaining atom in the "defect" dimer.

Second, we look at vacancy hopping between the up- and down-atom site in the "defect" dimer. In the calculation, we fix the x and y coordinates of the remaining atom at the certain values and only allow the z coordinate to move. The rest of atoms in the slab supercell are fully relaxed except the bottom Si layer and hydrogen atoms (used for the bottom layer passivation). The hopping barrier is calculated to be 0.4 eV.

Third, we calculate vacancy diffusion from the surface to the subsurface. The barrier is estimated to be 0.8 eV, with a return barrier of ~0.6 eV. Figure 3 shows intermediate configurations of the diffusing vacancy along the diffusion pathway: (i) the surface vacancy (a) starts moving along the (011) direction, (ii) the vacancy passes through the saddle point (b) of diffusion along a dimer row (as shown earlier), (iii) instead of hopping to the adjacent surface site, the vacancy continuously moves down to the subsurface, which involves a consorted motion of the atoms 2 and 12. The atom 12 moves up to restore a dimer with the remaining atom 2 while the atom 2 sinks to form a bond with the atom 20. The transition-state configuration is displayed in Fig. 1(c).

Since the diffusion will take place through the transition state of surface diffusion, it is likely that a surface vacancy mostly migrates to the adjacent surface site, rather than to the subsurface by overcoming an additional relatively large barrier of 0.5 eV. (Note that the barriers for vacancy diffusion along a dimer row and to the subsurface are 0.3 eV and 0.8 eV, respectively.)

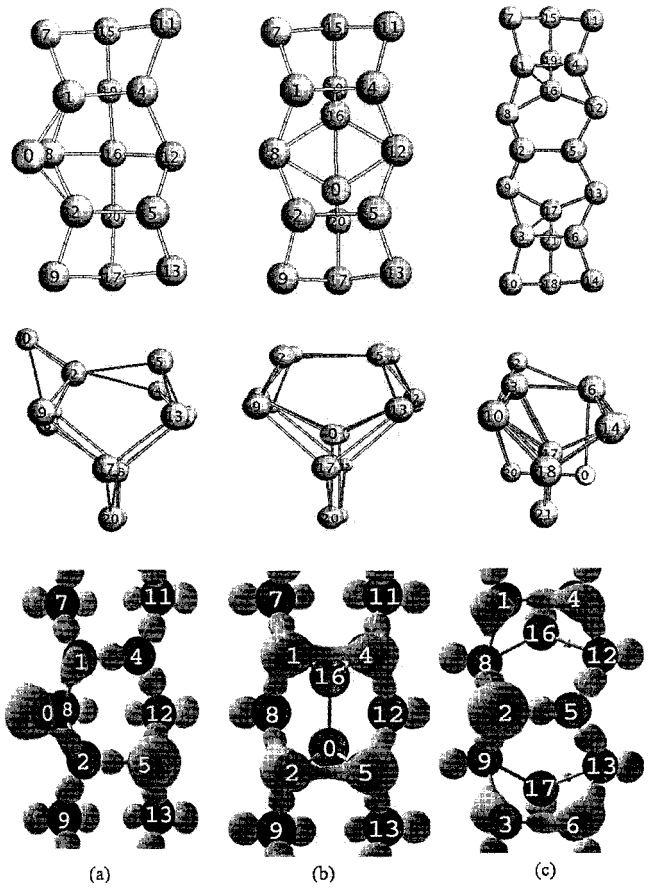

FIG. 5. (Color online) Top (top) and side (middle) view, together with ELF=0.86 isosurface maps (bottom), of adatom and sublayer interstitial defect structures. (a) adatom, indicated as 0, $d_{0\text{-}1}=d_{0\text{-}2}=2.40$ Å (b) (110)‖-split interstitial at the first sublayer. $d_{0\text{-}16}=2.39$ Å, $d_{1\text{-}4}=d_{2\text{-}5}=2.45$ Å, $d_{1\text{-}16}=d_{0\text{-}5}=2.50$ Å, $d_{16\text{-}4}=d_{0\text{-}2}=2.48$ Å. (c) $(110)_{\perp}$-split interstitial at the second sublayer, $d_{0\text{-}20}=2.84$ Å, $d_{1\text{-}4}=d_{3\text{-}6}=2.38$ Å, $d_{0\text{-}9}=d_{0\text{-}8}=2.52$ Å.

The complete energy diagram for vacancy diffusion up to the fourth subsurface layer is shown in Fig. 4. From the fourth to the third layer (state 3B), the diffusion barrier is estimated to be 0.13 eV. (The return barrier is 1.5 eV.) The diffusion shows a similar feature to the bulk diffusion.

Vacancy diffusion from the state 3B to the state 3A at the third layer requires overcoming an energy barrier of 0.6 eV. There is relatively large return barrier of 1.3 eV from the state 3A to the state 3B. This suggests that at moderate temperatures vacancies in the neutral state can be trapped at the third subsurface layer (state 3A). The surface atom 2 moves down and interacts with the atom 16. The atom 16 is dragged and pushed down to the position of the removed atom 20 and forms bonds with fourth layer atoms (which were originally connected to the atom 20). At the same time, the 16-8 and 16-12 bonds are broken, largely responsible for the relatively large diffusion barrier.

From the third layer site (state 3A) to the stable second layer site (state 2a), vacancy diffusion takes place through the metastable state (state 2B). The barrier of 0.4 eV from 3A to 2B may be associated with the breakage of the weak

TABLE II. Relative formation energy of a (various-state) neutral interstitial at different subsurface layers with respect to the fifth layer *H*-interstitial whose formation energy is set to be zero.

Layer	1	2	3	4	5
$(110)_{\perp}$		−1.3		−0.3	−0.06
$(110)_{\parallel}$	−3.0		−0.5		−0.06
H	−1.9	−0.4	−0.3	−0.2	0.0

16-19 bond. From the metastable to the stable state at the second layer, the vacancy can easily jump across with a very small barrier of 0.1 eV. (No bond breaking is associated with diffusion.)

Since the energy barriers for jumping across from the surface to the third layer are <1.0 eV and the formation energy differences are <0.2 eV, we expect that neutral vacancies will also be highly populated at the subsurface layers at moderated temperatures. However, given the far smaller formation energy of missing dimers, most vacancies will eventually remain in the form of missing dimers.

B. Neutral interstitials

Table II shows the total energy variation as a function of the distance of an interstitial from the surface. Here, we only present the energies of the most stable state at each layer. The total energy increases very rapidly as the interstitial is moved into a deeper subsurface layer. The difference in formation energy between the surface and the fourth layer interstitial is about 3.13 eV, indicating that neutral interstitials can be trapped (annihilated) at the surface, such as neutral vacancies. The significant energy gain of 3.0 and 1.3 eV at the first and second layers, respectively, with respect to the fifth layer (in which an interstitial shows a similar feature to bulk interstitials), is apparently ascribed to interstitial-surface interactions.

For the sake of reference, we first calculate the relative stability of bulk interstitials in the three different configurations. The result shows that the (110)-split and *H* states are energetically almost equivalent, and they are 0.29 eV more favorable than the *T* state, in good agreement with previous DFT studies.[30,31]

For an interstitial on the surface (i.e., adatom), the most stable site is on the side of a dimer row (in between two dimers) [Fig. 5(a)], consistent with previous DFT-LDA studies.[32] For an interstitial at subsurface layers, we consider two stable configurations; (110) split and hexagonal (*H*) states. Since surface reconstruction introduces the anisotropy to the system, we identify two (110) split states: (i) parallel to the dimer row, i.e., along the (011) direction [indicated as $(110)_{\parallel}$ split] and (ii) perpendicular to the dimer row, i.e., along the (011) direction [$(110)_{\perp}$ split]. The results are summarized in Table II.

At the first subsurface layer, the (110)-split state appears to be unstable due to strain induced by surface reconstruction. Upon geometry relaxation, with an initial position at the (110)-split site, the interstitial slides to the *H* site at between the first and second layers.

At the second layer, as shown in Fig. 5(b), the $(110)_{\parallel}$-split state turns out to be very stable. This state is only 0.2 eV less favorable than the most stable adatom state and 1.0 eV more stable than the *H* site in between the first and second layers. At the state, two adjacent dimers, 1-4 and 2-5, are symmetrized. Given such low formation energy, we expect that a large fraction of neutral interstitials would stay at the second subsurface layer as well.

At the third layer, the $(110)_{\perp}$-split state appears to be most favorable, about 0.8 eV more stable than the *H* state (between the second and third layers). As shown in Fig. 5(c), two Si atoms, 20 and 0 (inserted interstitial), share a lattice site while interacting with the second layer atoms 8, 9, 12, and 13. The 16-20 and 17-20 bonds are broken and the atoms 16 and 17 undergo an outward relaxation. They are stabilized by interacting with the symmetrized dimers 1-4 and 3-6, respectively.

At the third and fourth layers, the surface effect dwindles substantially. The difference in the relative formation energy between the (110) split and the *H* state decreases to 0.2 and 0.06 eV at the third and fourth layer, respectively. The overall formation energies are very close to those at the bulk.

IV. SUMMARY

The structure, energetics, and bonding of neutral vacancies and interstitials on the clean Si(001) surface and its subsurface layers are examined using first principles quantum mechanics calculations (density functional theory and quantum theory of "atoms in molecules"). We also present the diffusion pathways and barriers of vacancies at the vicinity of the surface.

We find that the formation energy of vacancies (interstitials) at the surface is about 2.4 eV (3.1 eV) lower than that at the fifth subsurface layer in which the intrinsic defects show a similar characteristic to the bulk ones. It appears that both vacancies and interstitials at the neutral state are unstable at the first subsurface layer such that they migrate to either the surface or the second subsurface layer immediately. We identify the very stable states of vacancies at the second and third subsurface layers, with the formation energy of only ≈ 0.2 eV greater than the surface one. Interstitials are also found to exist very stably at the second and third subsurface layers, with the formation energies of about 3.0 and 1.0 eV lower than the fifth layer one, respectively. Beyond the third layer, the surface proximity effect dwindles rapidly. The significant stabilization at the subsurface layers is mainly attributed to (i) the reduction of dangling bonds in the subsurface layers as a result of rearrangement of surface atoms and (ii) the delocalization of electrons on the local surface. It is likely that the strain induced by surface reconstruction plays a minor role in determining the relative stability of defects.

Our calculations also predict that the barriers for vacancy diffusion across the surface and subsurface layers are less than 0.4 and 0.8 eV, respectively. This suggests that neutral vacancies can easily jump across in the vicinity of the surface at elevated temperatures. Given the relatively small difference in formation energy between the surface and the sub-

surface layers, we expect that a large fraction of neutral vacancies would remain within the third subsurface layers until they form far more stable missing dimers.

In this study, we only consider intrinsic defects at the charge neutral state. We suspect the behavior of charged defects would be different from the neutral ones.

ACKNOWLEDGMENTS

G.S.H. acknowledges the Welch Foundation (Grant No. F-1535) for their partial financial support. Our calculations were performed using supercomputers in the Texas Advanced computing center at UT-Austin.

*Electronic address: anupam@uts.cc.utexas.edu
†Electronic address: gshwang@che.utexas.edu

[1] R. J. Hamers and Kohler, J. Vac. Sci. Technol. A **7**, 2854 (1989).
[2] R. J. Hamers, R. M. Tromp, and J. E. Demuth, Phys. Rev. B **34**, 5343 (1986).
[3] T. Aruga and Y. Murata, Phys. Rev. B **34**, 5654 (1986).
[4] Z. Y. Zhang and H. Metiu, Phys. Rev. B **48**, 8166 (1993).
[5] F. H. Stillinger and T. A. Weber, Phys. Rev. B **31**, 5262 (1985).
[6] K. C. Low, H. S. Lim, and C. K. Ong, J. Phys.: Condens. Matter **6**, 9551 (1994).
[7] P. Hohenberg and W. Kohn, Phys. Rev. **136**, B864 (1964); W. Kohn and L. J. Sham, Phys. Rev. **140**, A1133 (1965).
[8] G. Kresse and J. Furthmuller, VASP *the Guide* (Vienna University of Technology, Vienna, 2001); G. Kresse and J. Hafner, Phys. Rev. B **47**, RC558 (1993); G. Kresse and J. Furthmuller, Comput. Mater. Sci. **6**, 15 (1996); Phys. Rev. B **54**, 11 169 (1996).
[9] W. Kohn, A. D. Becke, and R. G. Parr, J. Phys. Chem. **100**, 12974 (1996).
[10] J. P. Perdew, K. Burke, and M. Ernzerhof, Phys. Rev. Lett. **77**, 3865 (1996).
[11] G. Kresse and J. Hafner, J. Phys.: Condens. Matter **6**, 8245 (1994).
[12] D. Vanderbilt, Phys. Rev. B **41**, 7892 (1990).
[13] H. J. Monkhorst and J. D. Pack, Phys. Rev. B **13**, 5188 (1976).
[14] H. Jonsson, G. Mills, and K. W. Jacobsen, in *Classical and Quantum Dynamics in Condensed Phase Simulations*, edited by B. J. Berne, G. Ciccotti, and D. F. Coker (World Scientific, Singapore, 1998), p. 385.
[15] G. Henkelman, B. P. Uberuaga, and H. Jónsson, J. Chem. Phys. **113**, 9901 (2000).
[16] R. F. W. Bader, J. Chem. Phys. **73**, 2871 (1980); R. F. W. Bader and H. Essen, *ibid.* **80**, 1943 (1984); R. F. W. Bader, *Atoms in Molecules: A Quantum Theory* (Oxford University Press, Oxford, 1960).
[17] B. Silvi and A. Savin, Nature (London) **371**, 683 (1994); A. D. Becke and K. E. Edgecombe, J. Chem. Phys. **92**(9), 5397 (1990); B. Silvi, J. Phys. Chem. A **107**(17), 3081 (2003).
[18] D. J. Chadi, Phys. Rev. Lett. **43**, 43 (1979).
[19] N. Roberts and R. J. Needs, Surf. Sci. **236**, 112 (1990); J. E. Northrup, Phys. Rev. B **47**, 10032 (1993); J. Fritsch and P. Pavone, Surf. Sci. **344**, 159 (1995).
[20] A. Redondo and W. A. Goddard III, J. Vac. Sci. Technol. **21**, 344 (1982); Z. Jing and J. L. Whitten, Surf. Sci. **274**, 106 (1992).
[21] G. S. Hwang and W. A. Goddard, Phys. Rev. B **65**, 233205 (2002).
[22] T. Uda and K. Terakura, Phys. Rev. B **53**, 6999 (1996).
[23] G. D. Watkins, in *Defects and Their Structure in Non-metallic Solids*, edited by B. Henderson and A. E. Hughes (Plenum, New York, 1976), p. 203; G. D. Watkins, in *Deep Centers in Semiconductors*, edited by S. T. Pantelides (Gordon and Breach, New York, 1986), p. 147.
[24] M. I. J. Probert and M. C. Payne, Phys. Rev. B **67**, 075204 (2003).
[25] L. J. Munro and D. J. Wales, Phys. Rev. B **59**, 3969 (1999).
[26] O. Sugino and A. Oshiyama, Phys. Rev. Lett. **68**, 1858 (1992).
[27] O. Pankratov, H. Huang, T. Diaz delaRubia, and C. Mailhiot, Phys. Rev. B **56**, 13 172 (1997).
[28] M. J. Puska, S. Poykko, M. Pesola and R. M. Nieminen, Phys. Rev. B **58**, 1318 (1998).
[29] T. Kirichenko, G. S. Hwang, and S. K. Banerjee, Surf. Sci. **555**, 187 (2004).
[30] R. J. Needs, J. Phys.: Condens. Matter **11**, 10 437 (1999).
[31] K. Kato, J. Phys.: Condens. Matter **5**, 6387 (1993).
[32] G. Brocks, P. J. Kelly and R. Car, Phys. Rev. Lett. **66**, 1729 (1991).